The synchrotron powder diffractometer at beamline B2 at HASYLAB/DESY: status and capabilities

Michael Knapp,* Carsten Baehtz, Helmut Ehrenberg and Hartmut Fuess

Darmstadt University of Technology, Institute for Materials Science, Germany. E-mail: mknapp@tu-darmstadt.de

The synchrotron powder diffraction beamline B2 at HASYLAB/DESY is described. The beamline is capable of high-resolution powder diffraction as well as time-resolved studies and offers several sophisticated ancillary equipments for special applications. A newly developed image-plate system allows for kinetic studies with good resolution in the minutes range. Numerous sample environments allow for various standard applications including structure solution, kinetic studies and *in situ* observations under flexible and well defined conditions. Representative examples are shown for these setups, which are also supported for experiments of external users.

Keywords: powder diffraction; *in situ* diffraction; high resolution.

1. Introduction

The powder diffractometer at beamline B2 at HASYLAB/DESY was built in 1988 at the synchrotron storage ring DORIS II (now DORIS III), and after a one-year shutdown period has been working since 1991, dedicated to user's applications. It is designed for diffraction from polycrystalline samples, including high angular resolution, resonant and time-resolved powder diffraction, texture and stress analyses and grazing-incidence measurements. The basic instrumental setup has already been reported (Arnold *et al.*, 1989; Pennartz, 1992; Loechner *et al.*, 1993), but numerous changes and improvements require an update of this description. All components of the beamline are now highly integrated and can be automatically controlled from a workstation. This allows the experimentalist to record complex measurements with little prearrangement. In the following the main components of the instrument are presented, and the capabilities of the different sample environments are demonstrated by selected examples.

2. Basic components

2.1. Radiation source

DORIS III is a dedicated source for synchrotron radiation of the second generation operated with positrons at an energy of 4.45 GeV (Brefeld *et al.*, 1988; Brefeld & Kaul, 1999; Kaul & Brefeld, 2001). Besides nine wiggler beamlines, more than 30 experimental stations are situated at bending magnets with a critical energy of 16.04 keV. The vertical size and divergence of the positron beam at the beamline is σ_z = 0.316 mm and σ'_z = 51.6 µrad. A further description of the beam parameters and source sizes of the storage ring is given elsewhere (http://www-hasylab.desy.de/facility/doris/parameters, http://www-hasylab.desy.de/facility/doris/beamsizes). The powder diffractometer itself is situated at beamline B2 at a distance of approximately 40 m from the bending-magnet source.

2.2. Primary beam optics

Half way to the synchrotron source (approximately 20 m), two different X-ray mirrors can alternatively be inserted into the beam path. The mirrors are mounted in line and can be moved and adjusted independently. In addition, the direct unmirrored beam can be used. Insertion of one of the mirrors leads to a vertical offset of 250 mm of the diffractometer.

One mirror option is a Pt-coated cylindrical mirror (Knapp *et al.*, 2001) with a pneumatically adjustable curvature. The size of the mirror is 1000 mm × 110 mm × 110 mm (length × width × height) and the curvature can be varied from flat to a focusing geometry. At the optimum working point the mirror collimates the residual vertical divergence of the synchrotron beam to a parallel beam. The reduced divergence increases the angular resolution of the diffractometer and the full width at half-maximum (FWHM) of the reflections decrease, especially at high diffraction angles (Wroblewski, 1991). According to Wroblewski (1991) the reflection half-widths can be described by equation (1) by introducing an additional term Δ_P describing the broadening caused by a standard reference material,

$$\mathrm{FWHM}^2 = \Delta_A^2 + \Delta_P^2 + \left[\frac{\tan(\theta_A) - 2\tan(\theta)}{\tan(\theta_M)}\right]^2 \Delta_M^2 + \left[\frac{2\tan(\theta) - \tan(\theta_M) - \tan(\theta_A)}{\tan(\theta_M)}\right]^2 \Phi_V^2. \quad (1)$$

In (1) the other parameters are: Δ_A and Δ_M, the Darwin width or mosaicity of the analyser and monochromator crystals, respectively, and θ_A and θ_M, the Bragg angles of the respective crystals. Φ_V is the vertical divergence of the photon beam. Assuming identical monochromator and analyser crystals, the *uvw* parameters of the Caglioti formula can be derived from (1) leading to (2), (3) and (4),

$$u = 4\left(\Delta^2 + \Phi_V^2\right)/\tan^2(\theta_M), \quad (2)$$

$$v = -\left(4\Delta^2 + 8\Phi_V^2\right)/\tan(\theta_M), \quad (3)$$

$$w = 2\Delta^2 + \Delta_P^2 + 4\Phi_V^2. \quad (4)$$

In Fig. 1 the graph of this function is plotted together with the FWHM values of the standard reference material LaB_6 (SRM 660a) from the National Institute of Standards and Technology (NIST). The sample was measured in transmission-mode geometry at 1.1314 Å with a Ge (111) analyser crystal in front of the NaI scintillation counter and Ge

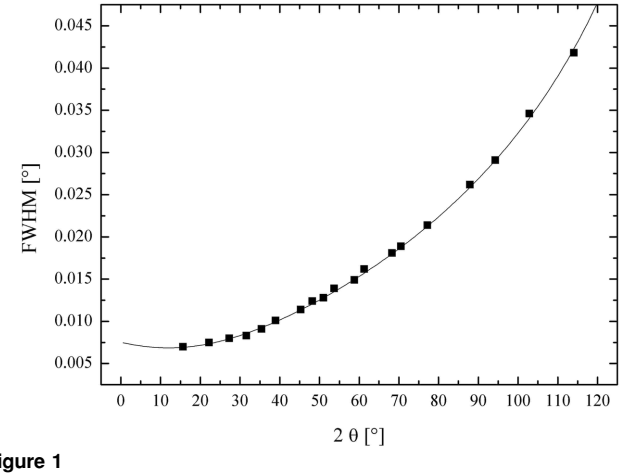

Figure 1
Full width at half-maximum of LaB_6 660a at room temperature and 1.1314 Å from single peak fits. The solid line is calculated from equation (1) with the values given in the text.

  DOI: 10.1107/S0909049504009367

Table 1
Comparison between the *uvw* parameters obtained by a least-squares fit of the Caglioti formula (5) and from the resolution function (1)–(4) with the values given in the text.

The angles are given in radians.

	u	*v*	*w*
Caglioti least-squares fit	$2.52\ (5) \times 10^{-7}$	$-4.6\ (6) \times 10^{-8}$	$1.5\ (1) \times 10^{-8}$
Equations (1) to (4)	2.57×10^{-7}	-5.44×10^{-8}	1.80×10^{-8}

(111) double flat-crystal monochromator. The graph was plotted using the following values:

$\Delta = \Delta_A = \Delta_M = 40$ μrad, the Darwin width of the analyser and monochromator crystals;

$\Delta_P = 115$ μrad, the broadening from the reference sample;

$\Phi_V = 20$ μrad, the vertical divergence of the collimated synchrotron beam;

$\theta_A = \theta_M = 10^\circ$, the monochromator angle.

Table 1 shows the values calculated from (1)–(4) and the *uvw* values obtained from a least-squares fit of the Caglioti formula, (5),

$$\mathrm{FWHM} = \left[u\tan^2(\theta) + v\tan(\theta) + w\right]^{1/2}. \quad (5)$$

The values obtained in both ways are very similar, and the *v* parameter always gives a negative contribution. The smallest achievable FWHM is about 0.006°, measured either with α-$RbAg_4I_5$ at a wavelength of λ = 1.2 Å (Knapp *et al.*, 2001) or LaB_6 (SRM 660a) standard reference material (λ = 1.1314 Å). The increase in half-width with 2θ leads to a value of about 0.042° at $2\theta = 114^\circ$, which is mainly attributed to the low vertical divergence of 20 μrad and is considerably lower than the typical value of 120–150 μrad that can be expected at a bending magnet at this facility.

Another mirror option is a toroidal-shaped Au-plated mirror (Doyle & Wroblewski, 1992). Its size is 1000 mm × 130 mm (length × width) and it focuses the horizontally divergent synchrotron beam onto the sample and thereby increases the intensity by a factor of ten. Hereby, the horizontal divergence of the beam is mapped into the vertical diffraction plane and the angular resolution in the wide-angle range is reduced. Fig. 2 shows a comparison of the half-widths of $LaAlO_3$ measured with a cylindrical-shaped and a toroidal-shaped mirror at a wavelength of 1.18 Å. The poorer resolution in the wide-angle range is obvious.

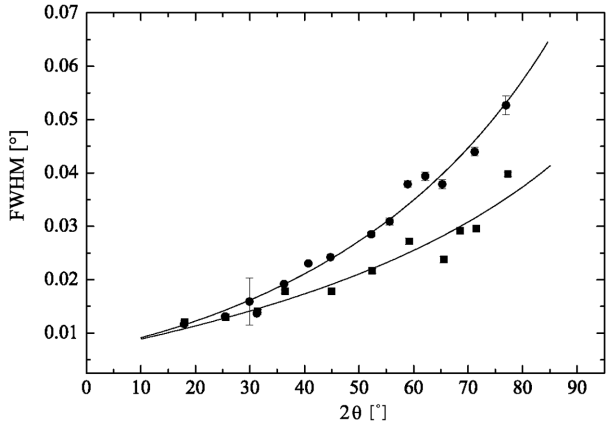

Figure 2
Comparison between the FWHM of $LaAlO_3$ measured with the toroidal (triangles) and cylindrical (squares) mirror at a wavelength of 1.18 Å.

Both mirrors are working under specular reflection, and an offset angle of about 0.74° has to be taken into account, which results in a difference of 250 mm in height for the diffractometer with respect to the direct beam. The accessible energy range is limited by the absorption edges of the coating materials ($\lambda_{min} = 1.12$ Å).

Two different monochromators are installed in a common helium-flushed vessel: one for the direct synchrotron beam and the other for the mirrored synchrotron beam. The vessel is located inside the hutch at a distance of 38 m from the source. A Si (111) double flat-crystal monochromator is used for the direct beam with an accessible wavelength range from 0.35 Å to 2.4 Å. The typical wavelength in this setting is 0.7 Å, which is in the range of the maximum flux of the storage ring. For the mirrored beam a double-crystal monochromator with Ge (111) crystals is used. Germanium increases the scattered intensity compared with silicon and conforms with its absorption edge to the coating materials of the X-ray mirrors. The accessible wavelength range is 1.12 Å to 2.4 Å.

Three independent slit systems are installed to control the beam size. The first is right in front of the X-ray mirrors defining the beam size and illumination of the mirror in use, and, hereby, defining the horizontal divergence allowed to enter the monochromator vessel. The second slit system after the monochromator defines the beam size on the sample, and the third, in front of the sample, blocks scattering from the beam-defining slit. Each slit system has four blades which can be aligned independently. Between the second and third slit system a NaI scintillation counter is placed at an angle of 90° to the beam. By means of scattering at a foil or from the helium atmosphere in the beam pipe, the incoming intensity can be monitored.

2.3. Diffractometer

The layout of the diffractometer provides the possibility of mounting even large sample environments like furnaces, a cryostat or a Eulerian cradle, and up to 50 stepping motors allow tailoring of the beamline to the needs of the user's experiments. The diffractometer itself (Fig. 3) mainly consists of three goniometers from HUBER Diffraktionstechnik GmbH (http://www.xhuber.com) with an angular resolution of 0.001° mounted on a lifting table. Two of them are attached concentrically, the third is situated opposite to them, and they can all be moved laterally to a maximum distance of 720 mm. In this way, a wide variety of sample environments can be adapted. The larger goniometer (Huber 480) carries a cantilever with the single counter mounted on two other goniometers (Huber 410). *Via* these goniometers, the counter can be aligned either with a set of parallel foils (Soller slits) or an analysing crystal. The two smaller goniometers (Huber 440) are designed to carry sample holders or the position-sensitive detector OBI. The lifting table can be moved vertically over more than 250 mm to position the experiment in either the direct or the mirrored synchrotron beam.

2.4. Detector systems

Three different types of detector are available: a scintillation single counter, a fourfold multidetector (Kaps, 2001) and an on-site readable position-sensitive image-plate detector (OBI) (Knapp *et al.*, 2004). The single counter consists of a NaI scintillator with embedded photomultiplier and optional slits, parallel foils, Ge (111) or Si (111) analyser crystal in front. Both height and angle of the crystal can be aligned and a tunable blade above the crystal absorbs contributions from the direct beam so that the Ge (111) crystal can be used at wavelengths below 0.5 Å. An absorber with aluminium foils of varying thicknesses in front of the counter allows for attenuation of

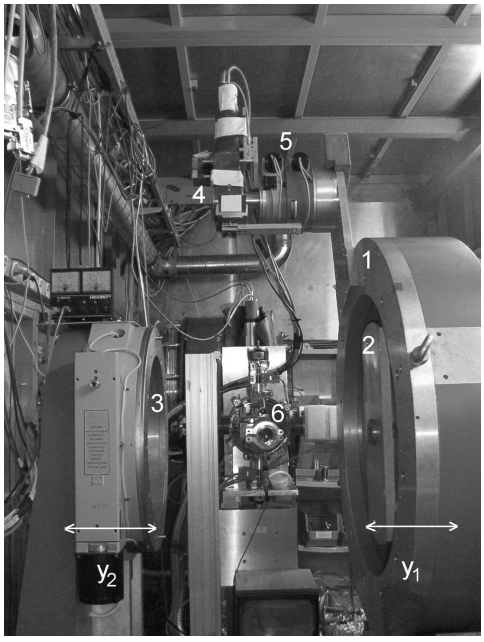

Figure 3
View of the diffractometer circles. The synchrotron beam enters the hutch from the back. The monochromator vessel is behind the diffractometer inside the hutch. 1: Huber circle 480 carrying the single counter. 2, 3: Huber circles 440 for sample environments or IP detector. 4: Single counter with analyser crystal and attenuator. 5: Two Huber circles 410 for counter alignment. The arrows marked y_1 and y_2 indicate the direction of lateral movement.

the scattered intensity (Pielaszek, 1999). The multidetector consists of a fan of four single counters with an angular spacing of 12.3° between them and either Si (111) flat crystals or Ge (111) channel-cut crystals in front of each single counter as analyser. Counters and analyser crystals are mechanically connected and can be moved simultaneously when the wavelength is changed. If the vacuum chamber is not used, collimators of 250 mm in length in front of each analyser reduce the background owing to air scattering. For fast measurements at medium resolution the on-site readable image-plate detector OBI can be operated complementarily to the single counter. The distance from image plate (IP) to sample is 345 mm and the spatial resolution of the detector is predominantly defined by the capillary diameter. Typically, a diameter of 0.3 mm is used, which leads to a reflection full width at half-maximum (FWHM) of 0.05° 2θ. This can be reduced to 0.03° using 0.1 mm capillaries. The maximum acceptance angle of the detector is 110° 2θ. At a wavelength of 0.7 Å the typical exposure time per pattern is in the range of minutes. Fig. 4 shows a pattern of a LaB_6/Si sample together with the Rietveld-calculated intensities and difference plot. The sample was filled into a 0.2 mm capillary and exposed for 30 s at a wavelength of 0.71 Å. With this detector the determination of thermal expansion, phase fractions and structural changes even in multiphase samples with low symmetry is possible. Likewise, the kinetics of the phase transitions have been traced (Ruschewitz *et al.*, 2003; Leineweber *et al.*, 2003).

2.5. Computer control

The experiment is controlled by a linux PC *via* a CAMAC bus system, using the *SPECTRA* programme package, developed and maintained by HASYLAB (Kracht, 2003*a*,*b*). Numerous AD and DA converter channels allow monitoring of parameters like beam position as well as control of measurement settings like high voltage. Peripheral devices are connected *via* GPIB bus, RS232 serial bus or ETHERNET. A second workstation with a Windows-NT operating system allows data inspection and treatment parallel to the experiment. Therefore a variety of software for Rietveld refinement or single-peak fit is installed.

3. Sample environments and representative applications

3.1. Ambient conditions

All standard diffraction geometries can be realized under ambient conditions: the Debye–Scherrer geometry with glass capillary (diameter 0.1–1.0 mm), the flat-specimen reflection geometry and the transmission-mode geometry. All setups have sample spinners. With these geometries, high-resolution measurements for structure determination (*e.g.* Herzberg *et al.*, 2001; Dinnebier *et al.*, 2002) and real structure analyses (*e.g.* Theissmann *et al.*, 2002; Ehrenberg, Theissmann *et al.*, 2002; Garcia-Martin *et al.*, 2004) are possible.

3.2. High temperature

Two sample environments for high-temperature applications exist at beamline B2. The first one is a capillary furnace from Stoe & Cie, type 0.65.3 (see http://www.stoe.com), which serves most of the experiments. In this furnace the capillary of diameter 0.3 mm is placed inside a drill hole in a graphite heating element. The capillary can then be rotated by using a rotating disc and the filling funnel of the capillary at one end. At the other end, just before the X-ray window, the capillary is fed through a 0.4 mm pinhole which acts as a bearing, minimizing eccentricity of rotation and ensuring that the sample remains in the centre of the X-ray window under rotation. This measure is essential for experiments using the IP detector to obtain regular reflection profiles. Owing to the horizontal mounting of the capillary and softening of the quartz glass at elevated temperatures, the highest accessible temperature is 1218 K. The heating element is flushed in a nitrogen atmosphere and the exit slit of the furnace covers an angular range of 0–90° 2θ for the diffracted intensity. In combination with the time-efficient OBI detector, changes can be monitored in small temperature steps, hereby revealing even tiny structural changes. Fig. 5 shows the anomalous behaviour of the *c*/*a* ratio in hexagonal $Fe_2Mo_3O_8$ between 573 and 873 K. The maximum deviation of the *c*/*a* ratio is smaller than 0.5‰, but clearly detected.

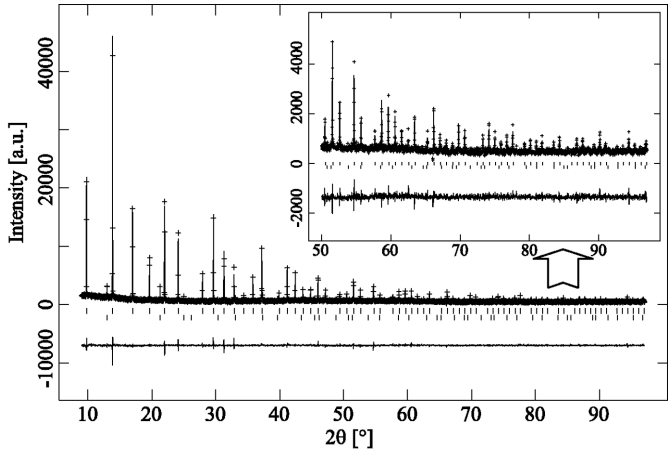

Figure 4
Measured and Rietveld-calculated data together with the difference plot of a LaB_6/Si sample in a 0.2 mm capillary measured with the OBI detector at a wavelength of 0.71 Å. Exposition was 30 s.

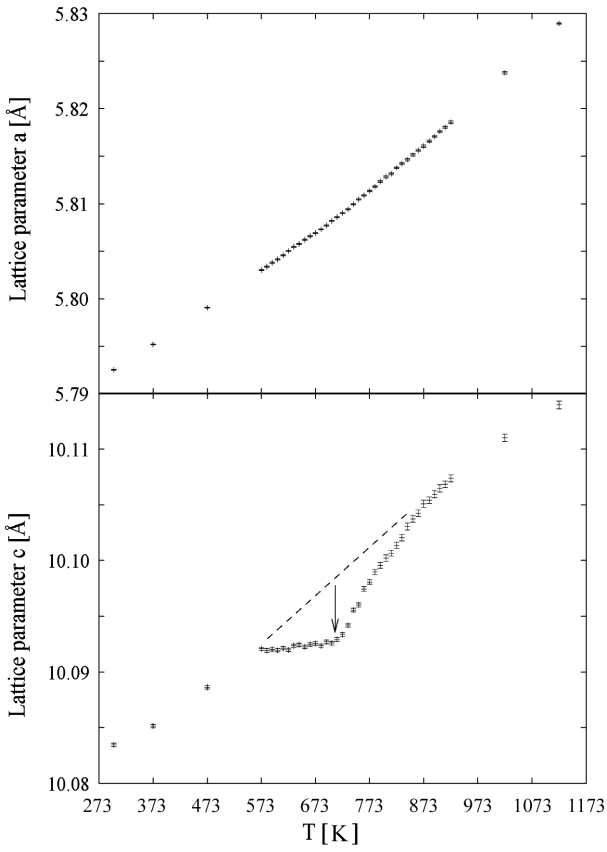

Figure 5
$a(T)$ (top) and $c(T)$ (bottom) for $Fe_2Mo_3O_8$ as obtained from Rietveld refinements, based on 41 data sets measured in 5 h using the OBI detector in combination with the Stoe capillary furnace.

In the temperature range between about 600 K and 2500 K a halogen mirror furnace with four symmetric 150 W halogen lamps powered by a DC voltage source is available. It is an enhancement of a device previously described by Schneider (1993). The furnace operates in air and the samples are typically free-standing ceramics or are filled in corundum or MgO capillaries mounted on a rotatable goniometer head. The lamp holder with the four water-cooled lamps is guided by a linear bearing and can be moved out of the beam to mount and dismount the goniometer head. Additionally, a type B thermocouple can be fixed onto the slide bar with the tip of the thermocouple inside the furnace to control the temperature up to 1673 K. Fig. 6 shows a schematic drawing of the furnace.

In both devices the temperature is controlled by a thermocouple, type K and type B, respectively. Systematic deviations in temperature have to be determined by calibrating with an adequate standard material after setup and alignment. Because of ageing of the halogen lamps the use of an internal standard in the mirror furnace is recommended for accurate temperature measurement. This can usually be accomplished by the corundum or MgO sample container or Pt paste. In both setups the temperature can be set remotely by a EUROTHERM controller.

3.3. Low temperature

The low-temperature device is a He closed-cycle cryostat from Cryophysics with a silicon diode as temperature sensor and a PID control circuit. It was adapted for powder diffraction applications and allows for a controlled gas atmosphere in the sample chamber (Ihringer & Koester, 1993). The cryostat works either in reflection or capillary geometry, both with sample spinner. The accessible temperature ranges from 10 to 330 K. In reflection geometry the powdered sample is glued onto a Si (711) low-background wafer and temperature is equilibrated in a low-pressure helium atmosphere. In order to make the cryostat compatible with the OBI detector, a capillary spinner with magnetic gear was introduced. Additionally, the whole cryostat can be vertically aligned with a motor-driven translation. This is necessary in order to compensate for the shrinking of the copper cold hat during cooling. In capillary geometry (Fig. 7) the powder has to be filled in sealed capillaries with diameters of 0.3–1.0 mm and length 30–35 mm. The capillaries are glued into a 15 mm long brass tube and plugged into the magnetically driven holder. In combination with scintillation counter and analysing crystal, high-resolution powder diffraction experiments can be performed (*e.g.* Ehrenberg, Dincer *et al.*, 2002; Ehrenberg *et al.*, 2004). When using the OBI detector, a large contribution from the Kapton shieldings to the background is found. This might be reduced by application of different or thinner window materials.

The combination of the cryostat with the high-resolution detector mode allows subtle details of structural transitions to be revealed. The evolution of the tetragonal (103) and (211) reflections of LiIn

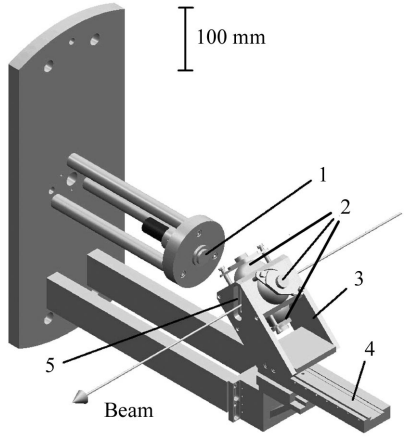

Figure 6
Schematic drawing of the halogen-mirror furnace. 1: Screw-mount for the goniometer head. 2: Halogen lamps. 3: Lamp holder. 4: Linear slide bar. 5. Exit window for the scattered beam (−10 to +38°). The trajectory of the synchrotron beam is also shown.

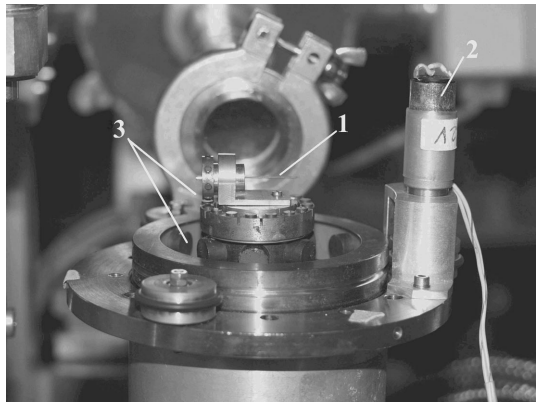

Figure 7
Photograph of the cryostat without shieldings. 1: Capillary with the sample. 2: Driving motor for the sample spinner. 3: Contactless magnetic gear.

into the cubic (311) reflection is shown as an example in Fig. 8 during the phase transition from $I4_1/amd$ to $Fd\bar{3}m$ (Ehrenberg, Pauly *et al.*, 2002). The coexistence of the tetragonal low-temperature and the cubic room-temperature structures over a wide temperature range is revealed as well as the discontinuity in the lattice parameters during this first-order transition (Fig. 9).

3.4. Precise sample positioning (Eulerian cradle)

For precise sample alignment a Eulerian cradle (Huber 513) with *xyz* stage can be mounted on the diffractometer. The maximum sample height is restricted to 55 mm. The cradle is working with the single counter only and offers the possibility for either texture and strain measurements or grazing-incidence diffraction and reflectometry (Rafaja *et al.*, 2004).

3.5. Vacuum chamber and resonant diffraction

For measurements with low background or at long wavelength from 1.8 to 2.4 Å a vacuum chamber for capillary geometry is provided (Gierlotka *et al.*, 1998). To avoid air scattering the residual pressure is kept below 100 Pa and the 2θ angles cover the range from -5 to 130° with a dead region between 62 and 65° owing to the shadow of a stabilizing pin. Nevertheless, this narrow region also becomes accessible by tilting the vacuum chamber by $\pm 1.5^\circ$. The chamber matches to either the single counter or the multidetector. Additionally, a special holder for image plates is available. In this case two IPs are mounted in line and have to be scanned off-site using a Storm 820 image-plate scanner (Molecular Dynamics). With this setup, both the dispersion corrections f' and f'' in $Er_5Re_2O_{12}$ (Ehrenberg *et al.*, 2000) at the Er L_{III} absorption edge (8.4 keV) and the site-specific electronic structure of Pr in $Pr_{1+x}Ba_{2-x}Cu_3O_{7-\delta}$ (Staub *et al.*, 2001) were determined. The very high absorption coefficients of the sample near the Pr L_{III} edge of about 6 keV requires exposure times of several minutes or even hours. For this type of experiment, good counting statistics and therefore low contributions from air scattering are essential. Structure refinements simultaneously based on several data sets at different wavelength allow for a very precise determination of thermal displacement factors. However, a sophisticated treatment of the energy-dependent absorption correction is a precondition for such a combined analysis (Ehrenberg *et al.*, 2000).

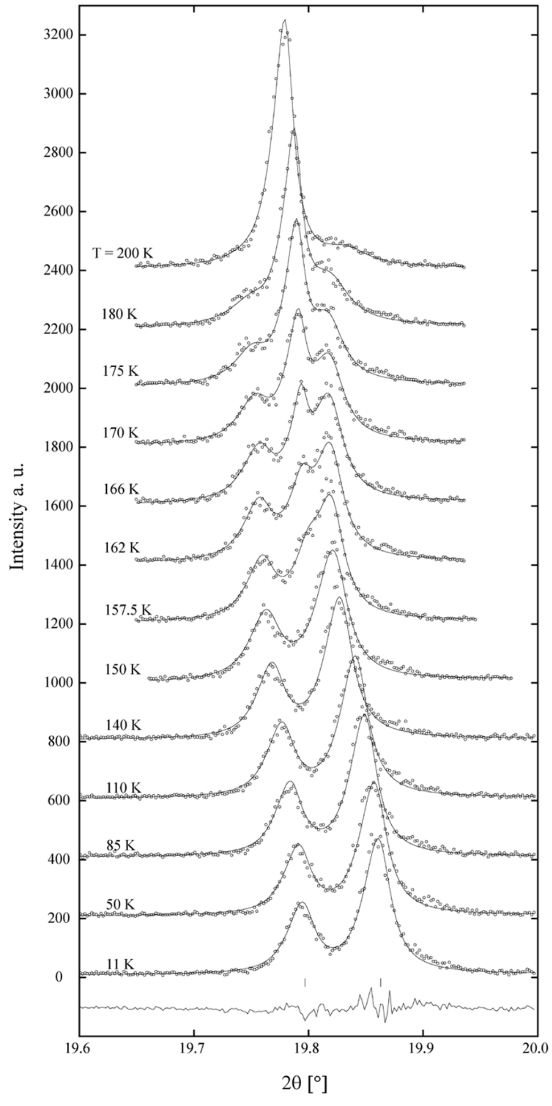

Figure 8
Section of the diffraction patterns of LiIn, recorded at different temperatures. Below 150 K only a shift of reflection positions is observed owing to thermal expansion, but an additional reflection from the onset of the cubic structure is observed at 157.5 K, increasing in intensity with temperature.

3.6. Electric field

For diffraction with high applied electric fields, a sample holder in reflection geometry is provided. A maximum bipolar voltage of 3 kV can be set from the main computer. The sample is disc-shaped, 10–15 mm in diameter and with a thickness of up to 1 mm. It is situated on top of an electrode with the second electrode sputtered on its upper side. With this setup, piezoelectric domain switching in PZT ceramics has been studied (Reszat *et al.*, 2001).

3.7. Uniaxial pressure

Uniaxial stress can be applied on samples like PZT ceramics with a size of 12 mm × 4 mm and thickness 1.9 mm. The holder is constructed as a steel frame. The sample is clamped between poles and the load is applied by means of a screw. Additionally, the pressure can be varied in a small range by expansion of a piezo stack actuator (PI 845) of up to 90 µm. The applied pressure is measured with a Kistler 9211 quartz pressure-sensor.

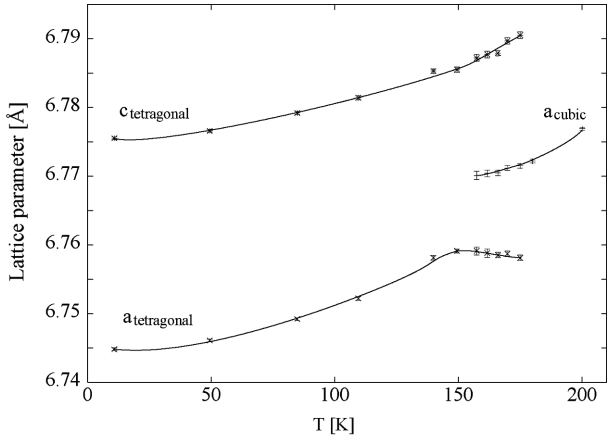

Figure 9
Temperature dependence of the LiIn lattice parameters during heating. A coexistence of both the tetragonal and the cubic phase is clearly seen. The lines are guides for the eyes.

3.8. Hydrogen loading

Two cells for the loading of materials with hydrogen are supported from an external user group: one for hydrogen gas loading of nanoparticles (Pundt *et al.*, 2002) and the other for electrochemical hydrogen loading of metallic layers embedded in KOH solution. With these cells the influence of hydrogen loading on the structure of the materials and the formation of different phases can be followed. The gas-loading cell consists of a tube of diameter 15 mm with mylar-foil windows. It can be evacuated and filled with a hydrogen atmosphere with defined pressure. In the electrochemical loading cell the sample is inside a Teflon sample holder and surrounded by potassium hydroxide solution, which can be pumped into and out of the reaction chamber (Dornheim, 2002). With these two cells the effect of hydrogen loading on the structure of the host system can be studied *in situ*, depending on gas pressure and the pH value of the electrolyte, respectively.

3.9. *In situ* investigations of charging and discharging of batteries

Structural changes during charging and discharging of battery materials are examined with an *in situ* loading cell in transmission geometry (Fig. 10). The electrodes and electrolytes are arranged in a sandwich structure and fixed in a frame made of PVC, which can be clamped into a holder (Fig. 11). Sample rotation is restricted by the wire connections between the cell and VMP potentio-galvanostatic device (VMP 60, Perkin-Elmer). Therefore, almost complete rotations are applied in an oscillating mode with turning points defined by sensors. This improves the grain statistics during the measurement. A detailed description of this loading cell and first results are published elsewhere (Baehtz *et al.*, 2004).

4. Conclusion

The powder diffraction beamline B2 at HASYLAB/DESY is a state-of-the-art instrument either for high-resolution powder diffraction or kinetic studies. Various sample environments allow versatile tailoring of experiments. The high-resolution setup allows measurements close to the theoretical resolution limit and is supplemented by a position-sensitive image-plate detector. In most setups both detector systems can be used complementarily, which offers the possibility of additional full-pattern measurements with medium resolution on a time scale of minutes. The latest developments will be presented on the world wide web (http://www-hasylab.desy.de/facility/experimental_stations/stations/B2.htm).

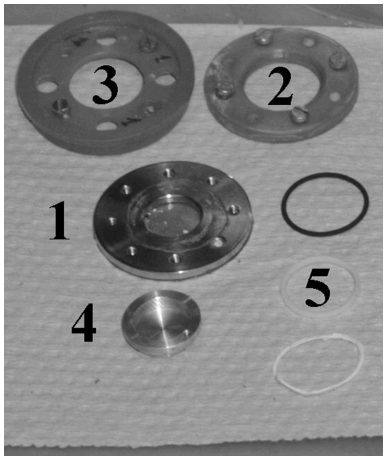

Figure 10
Photograph of the loading cell. 1: Anode contact (steel) with beam exit window (Kapton foil). 2: Cell support (PVC). 3: Cell holder (PVC). 4: Beam entrance window (aluminium). 5: Sealing (PTFE).

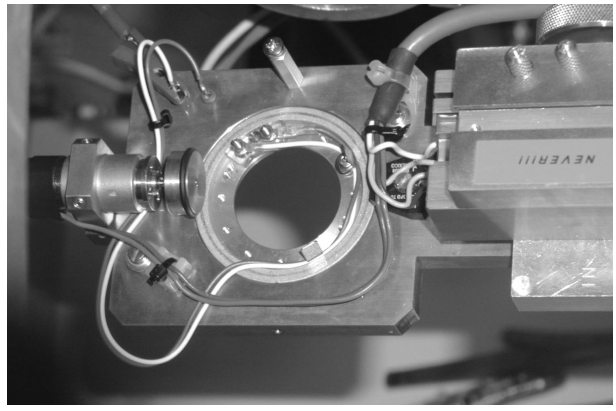

Figure 11
Photograph of the holder for the loading cell. The cell can be clamped into the holder and oscillated or rotated.

Financial support from the Bundesministerium für Bildung und Forschung (Germany) under grant Nos. 05KS1RDA9 and 05SM8RDA is gratefully acknowledged. We also thank HASYLAB for technical and advisory support, especially W. Ternes, T. Wroblewski and T. Kracht. For collaboration in development and installation of sample environments and reconstruction of the beamline we would like to thank A. Berghaeuser and C. Heidmann (University of Hamburg), J. Ihringer and W. H. Kaps (University of Tübingen), A. Pundt and M. Dornheim (University of Göttingen), Ju. Schneider (LMU, München), J. Reszat and H. Kungl (TU Karlsruhe) and R. Pielaszek (HPRC, Polish Academy of Sciences).

References

Arnold, H., Bartl, H., Fuess, H., Ihringer, J., Kosten, K., Loechner, U., Pennartz, P. U., Prandl, W. & Wroblewski, T. (1989). *Rev. Sci. Instrum.* **60**, 2380–2381.
Baehtz, C., Buhrmester, T., Bramnik, N. N., Nikolowski, K., Ehrenberg, H. & Fuess, H. (2004). Submitted
Brefeld, W. & Kaul, O. (1999). *HASYLAB Annual Report*, pp. 27–28. HASYLAB, Hamburg, Germany.
Brefeld, W., Nesemann, H. & Rossbach, J. (1988). *Proceedings of the European Particle Accelerator Conference*, pp. 389–391. Singapore: World Scientific.
Dinnebier, R., Ibberson, R., Ehrenberg, H. & Jansen, M. (2002). *J. Solid State Chem.* **163**, 332–339.
Dornheim, M. (2002). PhD thesis, University of Göttingen, Germany.
Doyle, S. E. & Wroblewski, T. (1992). *HASYLAB Annual Report*, pp. 621–622. HASYLAB, Hamburg, Germany.
Ehrenberg, H., Dincer, I., Elmali, A., Elerman, Y. & Fuess, H. (2002). *Solid State Commun.* **124**, 429–432.
Ehrenberg, H., Knapp, M., Hartmann, T., Fuess, H. & Wroblewski, T. (2000). *J. Appl. Cryst.* **33**, 953–957.
Ehrenberg, H., Pauly, H., Hansen, T., Jaud, J.-C. & Fuess, H. (2002). *J. Solid State Chem.* **167**, 1–6.
Ehrenberg, H., Pauly, H., Knapp, M., Groebner, J. & Mirkovic, D. (2004). *J. Solid State Chem.* **177**, 227–230.
Ehrenberg, H., Theissmann, R., Gassenbauer, Y., Knapp, M., Wltschek, G., Weitzel, H., Fuess, H., Herrmannsdoerfer, T. & Sheptyakov, D. (2002). *J. Phys. Condens. Matter*, **14**, 8573–8581.
Garcia-Martin, S., Alario-Franco, M. A., Ehrenberg, H., Rodriguez-Carvajal, J. & Amador, E. (2004). *J. Am. Chem. Soc.* **126**, 3587–3596.
Gierlotka, S., Palosz, B., Pielaszek, R., Stel'makh, S., Doyle, S. & Wroblewski, T. (1998). *Mater. Sci. Forum*, **278/281**, 106–109.

Herzberg, O., Ehrenberg, H., Kitchin, S. J., Harris, K. D. M. & Epple, M. (2001). *J. Solid State Chem.* **156**, 61–67.
Ihringer, J. & Koester, A. (1993). *J. Appl. Cryst.* **26**, 135–137.
Kaps (2001). *The Multiple-Detector System for the powder diffractometer B2 (HASYLAB/DESY)*, http://www.uni-tuebingen.de/uni/pki/Multidetector.
Kaul, O. & Brefeld, W. (2001). *HASYLAB Annual Report*, pp. 73–74. HASYLAB, Hamburg, Germany.
Knapp, M., Ehrenberg, H., Fuess, H., Hahn, U., Hesse, M., Schulte-Schrepping, H. & Wroblewski, T. (2001). *Nucl. Instrum. Methods*, A**467**/**468**, 291–293.
Knapp, M., Joco, V., Baehtz, C., Brecht, H. H., Berghaeuser, A., Ehrenberg, H., von Seggern, H. & Fuess, H. (2004). *Nucl. Instrum. Methods*, A**521**, 565–570.
Kracht (2003*a*). *SPECTRA, A Program Package for the Analysis and Presentation of Data*, http://www-hasylab.desy.de/services/computing/spectra/spectra.html.
Kracht (2003*b*). *On-Line, A Program Package for Data Acquisition and Beamline Control at HASYLAB*, http://www-hasylab.desy.de/services/computing/online/online.html.
Leineweber, A., Mittemeijer, E. J., Knapp, M. & Baehtz, C. (2003). *Mater. Sci. Forum*, **443**/**444**, 247–259.
Loechner, U., Pennartz, P. U., Miehe, G. & Fuess, H. (1993). *Z. Kristallogr.* **204**, 1–41.
Pennartz, P. U. (1992). *J. Appl. Cryst.* **25**, 571–577.
Pielaszek (1999). *Attenuator Controller user's manual*, http://www.unipress.waw.pl/~pielasze/desy/attenuator/manual.html.
Pundt, A., Dornheim, M., Guerdane, M., Teichler, H., Ehrenberg, H., Reetz, M. T. & Jisrawi, N. M. (2002). *Eur. Phys. J*, D**19**, 333–337.
Rafaja, D., Ebert, J., Miehe, G., Martz, N., Knapp, M., Stahl, B., Ghafari, M., Hahn, H., Fuess, H., Schmollngruber, P., Farber, P. & Siegle, H. (2004). *Thin Solid Films.* In the press.
Reszat, J. T., Glazunov, A. E. & Hoffmann, M. J. (2001). *J. Eur. Ceram. Soc.* **21**, 1349–1352.
Ruschewitz, U., Baehtz, C. & Knapp, M. (2003). *Z. Anorg. Allg. Chem.* **629**, 1581–1584.
Schneider, J. (1993). *Adv. X-ray Anal.* **36**, 397–402.
Staub, U., Shi, M., Conner, A. G. O., Kramer, M. J. & Knapp, M. (2001). *Phys. Rev. B*, **63**, 134522.
Theissmann, R., Ehrenberg, H., Weitzel, H. & Fuess, H. (2002). *J. Mater. Sci.* **37**, 4431–4436.
Wroblewski, T. (1991). *Acta Cryst.* A**47**, 571–577.

 Received 19 February 2004 • Accepted 19 April 2004